MODELING OF OXYGEN CHEMISORPTION ON MICROPOROUS CARBONS

J. K. Floess
Department of Chemical Engineering
University of Illinois at Chicago
Chicago, IL

Keywords: microporous carbons; oxygen chemisorption; chemisorption kinetics

Introduction

The reaction of oxygen with carbon is believed to involve the dissociative adsorption of oxygen on the carbon to form carbon-oxygen surface complexes and the subsequent desorption of these complexes to carbon monoxide, or in a more complex sequence of steps, to carbon dioxide. The oxygen chemisorption step is effectively irreversible in that desorption to oxygen apparently does not occur; instead, desorption involves the breaking of one or more carbon-carbon bonds in the solid and the formation of carbon oxides. Because the adsorption and desorption steps involve distinct chemical pathways, however, it is necessary to investigate each of these step independently in order to determine the overall energetics of the reaction. An objective of this study was to determine activation energies for the oxygen chemisorption step by analyzing chemisorption data on a microporous char in terms of a distributed activation energy model.

This paper discusses the modeling of oxygen chemisorption kinetics with the assumption that there is a distribution of activation energies for adsorption. Two different types of heterogeneous surfaces were considered: in one case, it was assumed that the surface has an a priori distribution of activation energies for adsorption whereas in the second case, it was assumed that the activation energy increases as a consequence of oxygen chemisorption (i.e., due to induced heterogeneity). For each model, the activation energy was assumed to vary linearly with coverage. Experimental data reported by Kelemen and Freund[1] and by Floess et al.[2] show that the activation energy for chemisorption, to a first approximation at least, increases linearly with oxygen coverage. Consequently, the proposed distribution does adequately represent available experimental data. Furthermore, the use of a linear distribution function allows the model equations to be solved analytically rather than numerically. The availability of analytical equations simplifies the problem of obtaining model parameters from experimental data, and finally, an analytical solution provides insight into the behavior of the solution that is not easily discernible from numerical results.

Experimental

In this study, oxygen chemisorption data on a microporous carbon were obtained in a series of isothermal adsorption runs at temperatures between 400 and 548 K and at oxygen partial pressures up to 1atm. Experimental data were obtained using a thermogravimetric analyzer. Gas compositions in the reactor were also monitored by leaking a small amount of gas to a quadrupole mass spectrometer. A detailed description of the experimental approach is given in reference (2).

Chemisorption data were obtained with Spherocarb that had been partially reacted to 5% conversion and then outgassed. Pretreatment of the char in this manner was found to substantially increase the amount of oxygen that could be chemisorbed at low temperatures. The experimental data, which are presented later, are reported on a normalized basis with respect to the maximum amount adsorbed, which was taken to be the amount adsorbed at conditions where the rate of gasification is negligible. This oxygen uptake, however, is significantly less than the amount of oxygen typically present on a char after partial gasification. In other words, with carbon conversion, the oxygen content increases significantly above the amount present when no conversion has yet occurred. Although the choice of a normalization factor for reporting experimental data is to a degree arbitrary, its value can affect the interpretation of the model results, as will be shown later.

Chemisorption Models

The first model assumes that there exists a continuous distribution of activation energies for adsorption. Here $\eta(\varepsilon)$ is the density of the distribution function, and $\eta(\varepsilon)\Delta\varepsilon$ is the fraction of total sites with an activation energy for adsorption between ε and $\varepsilon+\Delta\varepsilon$. The rate of adsorption on sites of energy ε is:

$$\frac{d[C(O)_\varepsilon]}{dt} = k_\varepsilon C_{O_2} (1 - \theta_\varepsilon) \qquad (1)$$

where $C(O)_\varepsilon$ is the concentration of adsorbed oxygen atoms on sites of energy ε; k_ε is the adsorption rate constant; C_{O_2} is the oxygen concentration; and θ_ε the fraction of sites of energy ε that are occupied. The reverse reaction is neglected in this equation since oxygen chemisorption is assumed to be irreversible, and the analysis is limited to the case of negligible gasification. Integration of (1) yields:

$$\frac{C(O)_\varepsilon}{C_{T_\varepsilon}} = \theta_\varepsilon = [1 - \exp(-\bar{k}_\varepsilon t)] \qquad (2)$$

where $\bar{k}_\varepsilon = k_\varepsilon C_{O_2} / C_{T_\varepsilon}$.

The total amount adsorbed is obtained by integrating equation (2) over the activation energy distribution:

$$\{C(O)\}(t) = C_t \int_{\varepsilon_*}^{\varepsilon^*} [1 - \exp(-\bar{k}_\varepsilon t)]\, \eta(\varepsilon)\, d\varepsilon \tag{3}$$

For a linear distribution function (i.e., the density of the distribution is equal to a constant), equation (3) may be integrated analytically to give:

$$\theta(t) = \frac{\{C(O)\}t}{C_t} = 1 - \eta_0 RT\, [E_1(\bar{k}^* t) - E_1(\bar{k}_* t)] \tag{4}$$

where E_1 is the exponential integral; $\eta_o = 1/(\varepsilon^* - \varepsilon_*)$; and $\bar{k}^*$ and $\bar{k}_*$ are the rate constants at ε^* and ε_*, respectively.

This equation may be differentiated to obtain the rate of oxygen chemisorption:

$$\frac{d\theta}{dt} = \eta_0 \frac{RT}{t} [e^{-\bar{k}^* t} - e^{-\bar{k}_* t}] \tag{5}$$

The rate equation for the second model, where it is assumed that surface heterogeneity is induced by oxygen chemisorption, is:

$$\frac{d[C(O)]}{dt} = k(\theta)\, C_{O_2} (1 - \theta) \tag{6}$$

Here $k(\theta)$ indicates the dependence of the adsorption rate constant on oxygen coverage. This model has been used by Tokoro et al.[3] to analyze desorption data and to obtain site energy distributions from experimental data in a comparatively straightforward manner.

For the case where ε varies linearly with θ:

$$\varepsilon = a\theta + b \tag{7}$$

equation (6) can be integrated to yield:

$$\int_0^\theta \frac{e^{a\theta/RT}}{(1 - \theta)}\, d\theta = k't \tag{8}$$

Here $k' = A_o \exp(-b/RT)\, C_{O_2}/C_t$

This integral may be evaluated to obtain its asymptotic behavior as $\{a/RT\} \rightarrow \infty$:

$$k't = \frac{RT}{a} \frac{e^{a\theta/RT}}{(1 - \theta)} \tag{9}$$

Equations (4) and (8) are intrinsic rate equations for oxygen chemisorption for each model. However, in applying these equations to experimental data it is necessary to correct for the effects of bulk phase mass transfer, intra-particle diffusion, and instrument response time on the observed kinetics. In this study the two principal effects were the instrument response time and and the bulk phase mass transfer resistance. (Although, as a rule of thumb, intra-particle diffusion will usually manifest itself before bulk phase diffusion, in this study this was not the case since the length scales for mass transport and intra-particle diffusion were widely different. Experimental measurements[2] confirmed that there was no effect of particle size on the chemisorption rates obtained in these experiments.)

The TGA used in the experiments had a characteristic response time of 3.4 sec. The response of the instrument to a step change in weight could be adequately fitted by a first order model (both first and second order response models were investigated).

The mass transfer coefficient was estimated from the correlations of Wigmans et al.[4] and of Treybal[5]. Both correlations yield a Sherwood number of approximately 4. over the temperature range of 300-800K and for a flowrate of 60 scc/min. However, because of the large temperature gradient in the furnace tube neither correlation is entirely valid for the actual flow conditions in the TGA. The Raleigh number for the gas flow in the furnace tube is estimated to be $3.x10^5$, and for this value, the flow in the tube is dominated by free convection[6]. In any case, the characteristic mass transfer time (at an oxygen partial pressure of 0.5 atm) is 1.0 s, so that instrument lag is the dominant resistance for the experiments reported here.

The bulk phase mass transport resistance can be incorporated in a straight forward manner into the model of Tokoro to give:

$$\frac{d\theta}{dt} = \frac{C_{o_2}^{\circ}}{\frac{1}{k_r(1-\theta)} + \frac{1}{k_m}} \tag{10}$$

where k_m is a mass transfer coefficient, $k_r = k(\theta)/C_t$, and $C_{o_2}^{\circ}$ is the bulk oxygen concentration. This equation can be integrated to give:

$$t = \frac{1}{k'} \int_0^{\theta} \frac{e^{a\theta/RT}}{(1-\theta)} \, d\theta + \frac{\theta}{k_m C_{o_2}^{\circ}} \tag{11}$$

For the distribution model no simple rate equation that includes the mass transfer resistance can be obtained.

Since the instrument response to a step disturbance is known, Duhamel's integral was evaluated to determine the actual uptake of oxygen recorded in the experiments:

$$\theta = \int_0^t \theta(s) \frac{1}{\tau} e^{-(t-s)/\tau} \, ds \tag{12}$$

where $\theta(s)$ is the amount of oxygen adsorbed as a function of time given by equation 4, 8, or 11 and τ is the instrument time constant. The integral was evaluated analytically by locally approximating $\theta(s)$ by a straight line over a time interval Δt_i. The results of the integration are presented in Figure 1. As shown, the adsorption curves obtained when the mass transfer resistance is also included in the calculations are not appreciably different from the case where this resistance is neglected. Consequently, the mass transfer resistance is neglected in comparing the results of each model, and equations (4) or (8) are used directly in equation (12).

Discussion

Calculations were done for different ranges of activation energies, which corresponds to different slopes for the activation energy distribution shown in Figure 2. It is likely, as shown by the dashed lines in the figure, that deviations from linearity occur at both extremes of the distribution. The deviation from linearity at the low activation energy end will not appreciably affect the results since chemisorption rates here are faster than can be measured experimentally under non-vacuum conditions. At the high end, it is assumed that the fraction of sites that deviate from the linear model and also contribute appreciably to the adsorption rate is small. Calculations were also done for two different values of the normalization factor.

Predicted isothermal adsorption curves at 400, 448, 498, and 548 K for two different activation energy ranges are shown in Figures 3 and 4. Both models give adsorption curves of a similar shape, and in fact, there is no basis for distinguishing between models. As a result, the choice of a model can be largely dictated by mathematical convenience. The model of Tokoro is advantageous when corrections for bulk phase mass transport or intra-particle diffusion need to be taken into account, and this model can be used in a straightforward manner to obtain a site distribution from experimental rate data by solving a set of n linear equations in m unknowns[3]. The unknowns are the pre-exponential factor and the constants in the function assumed for $\varepsilon(\theta)$. The principal disadvantage of this model is that the correct θ values for the experimental data must be known.

Changing the range of activation energies alters the rise of the individual adsorption curves and the spacing between individual curves. However, these differences in the shape of the curves are not very sensitive to a change in the activation energy range. (For the two sets of data shown, the pre-exponential factors differ by 10^6.) In general, lowering the activation energy range tends to increase the rise of the curve between the initial, approximately linear, part and the final amount adsorbed and tends to push the curves closer together and up toward $\theta=1$. This bunching effect is accentuated for data near $\theta=1$. If, however, a larger normalization factor is used in calculating θ, the isothermal adsorption curves remain approximately equally spaced and do not come together since now the curves never reach $\theta=1$. As a result, the determination of the correct activation energy range is more difficult since one can now only use the rise of the curves to discriminate between activation energy ranges.

The effect of oxygen partial pressure on the adsorption curves is shown in Figure 5. The predicted curves are in good agreement with experimental data[2] previously reported.

Experimental chemisorption data for Spherocarb are presented in Figure 6, where the data are compared to model predictions for an activation energy range of 12 to 32 kcal/mole. This range gave the best agreement with the data for the assumption of a linear variation in activation energy with oxygen coverage. Agreement between the data and the model is satisfactory, although the model predicts a more rapid initial increase in oxygen coverage than is exhibited by the data. This discrepancy may be because the linear distribution assumed in the calculations is not sufficiently accurate for representing the actual activation energy distribution with the necessary precision.

Conclusions

This paper examined kinetic models for oxygen chemisorption on two types of heterogeneous carbon surfaces. In each case, a linear variation in activation energy with oxygen coverage was assumed. The models include correction terms for the effects of bulk phase mass transport and instrument response on the observed kinetics.

It was found that the adsorption curves obtained from each model are essentially similar and that the use of one or the other can be largely dictated by computational convenience. For example, the Tokoro model can be regressed in a straightforward manner to obtain model parameters from the data and can be readily modified to include the effects of intra-particle diffusion or bulk phase mass transfer on the kinetics.

Based on an analysis of experimental chemisorption data, it is concluded that the activation energy for oxygen chemisorption on a microporous char is in the range of 12-32 kcal/mole. However, since model predictions are rather insensitive to the range of activation energies, experimental data at precise temperature intervals are needed to accurately determine the activation energy range for chemisorption kinetics.

The models can correctly account for the oxygen partial pressure dependence of the chemisorption data.

References

1. Kelemen S. R.; Freund, H. *Carbon*, 1985, 23, 723-729.
2. Floess, J. K.; Lee, K-J.; Oleksy, S. A. *Energy and Fuels*, 1991, 5, 133.
3. Tokoro, Y.; Uchijima, T.; Yoneda, Y. *J. of Catal.*, 1979, 56, 110.

3a. Tokoro, Y.; Misono, M.; Uchijima, T.; Yoneda, Y. *Bull. Chem Soc. Japan*, 1978, 51, 85.

4. Wigmans, T.; v. Cranenburgh, H.; Elfring, R.; Moulijn, J. A. *Carbon*, 1983, 21, 23.
5. Treybal, R. E. *Mass Transfer Operations*; McGraw-Hill: New York, 1980.
6. Eckert E. R.; Drake, R. M. *Analysis of Heat and Mass Transfer*; McGraw-Hill, New York, 1972.

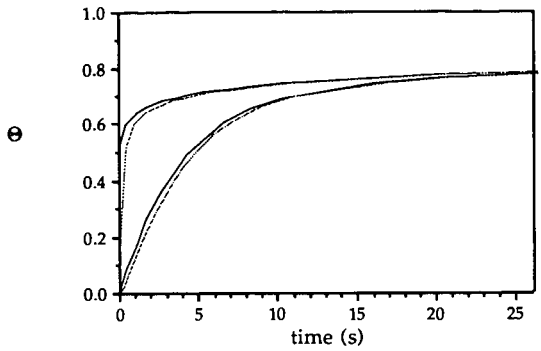

Figure 1. Effect of instrument response on chemisorption kinetics. Curves towards the left side of the graph are instrinsic kinetics; curves towards the right include instrument response; model of Tokoro: (- -) includes mass transfer resistance; (—) no mass transfer included.

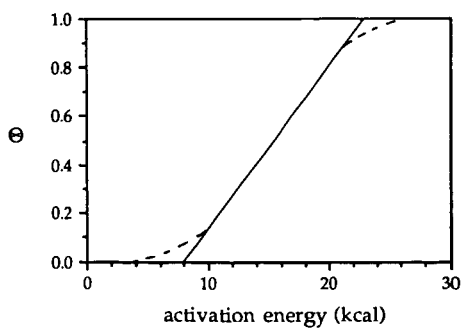

Figure 2. Activation energy distribution.

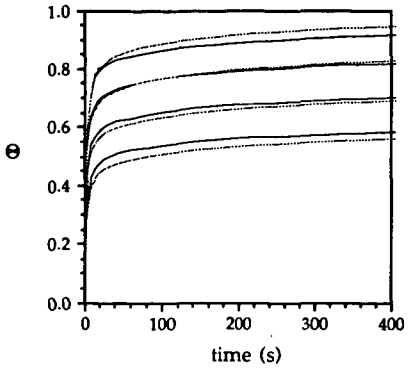

Figure 3. Predicted chemisorption curves at 400, 448, 498, 548 K, 0.5 atm oxygen partial pressure; activation energy range: 12.3 to 34.8 kcal; (---) distributed site model; (—) model of Tokoro.

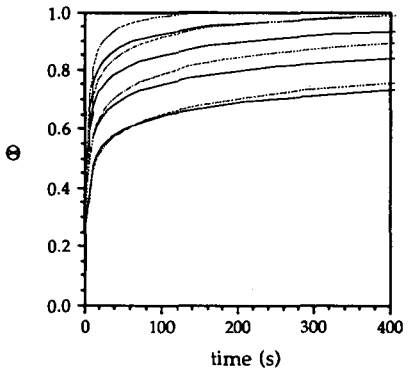

Figure 4. Predicted chemisorption curves at 400, 448, 498, 548 K, 0.5 atm oxygen partial pressure; activation energy range: 5.8 to 16.7 kcal; (---) distributed site model; (—) model of Tokoro.

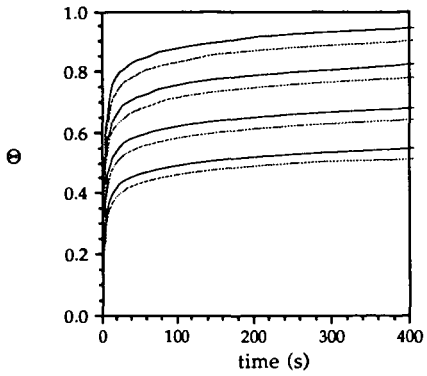

Figure 5. Model results for oxygen partial pressures of 0.5 atm (—) and 0.21 atm (---); site energy distribution model; activation energy range: 11.8 to 32.4 kcal.

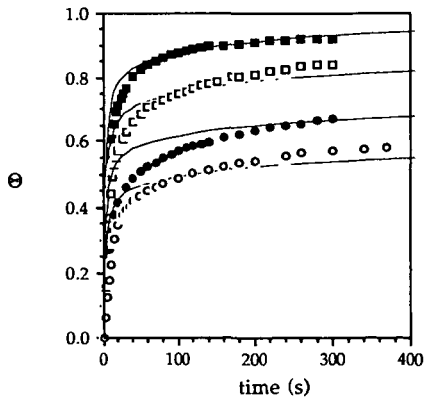

Figure 6. Comparision of chemisorption data at 400, 448, 498, and 548 K and 0.5 atm oxygen partial pressure to model results. Site energy distribution model; activation energy range: 11.8 to 32.4 kcal.